

Supersonic Drag Performance of Truncated Cones with Repetitive Energy Depositions

Takeharu Sakai^a

Department of Aerospace Engineering, Nagoya University,
Furo-cho, Chikusa-ku, Nagoya, Japan, 464-8603
tsakai@nae.nagoya-u.ac.jp

ABSTRACT

The drag performance of truncated cones in a supersonic flow of Mach number 2 with repetitive energy depositions is evaluated by using computational fluid dynamics. The calculated result shows a quasisteady flowfield: a virtual spike, which is supported by an axi-symmetric recirculation, is formed in front of the truncated cone. The recirculation is generated due to baroclinic interaction between a bow shock wave and a heated bubble produced by energy depositions. The reduction of the drag over the truncated cone is attributed to the virtual spike so formed. The time averaged drag of the truncated cone depends on the amount of deposited energy, repetition frequency and the area of a truncation surface. The averaged drag can be smaller than that of a sharp cone with the same apex angle, maintaining the energy savings due to drag reduction.

NOMENCLATURE

B	blast wave
D	instantaneous drag, N
D_0	drag without energy deposition, N
D_{0_ffc}	D_0 of flat-faced cylinder, N
D_{0_TM}	D_0 of cone with 30 degree nose angle calculated from Taylor-Maccoll solution, N
D_{av}	averaged drag, N
f	repetitive frequency, Hz
L	low density core
M	Mach number
O	oblique shock wave
Q	deposited energy, J
q_0	deposited power per unit volume, W/m ³
r	radial coordinate, m
r_0	radius of absorbed energy volume, m ³
s	distance upstream of blunt body to energy deposition position, m
t	time, s
V_∞	freestream velocity, m/s
v	volume, m ³
v_0	spherical volume for energy absorption, m ³
x	axial coordinate, m
x_0	x coordinate value for energy deposition, m
ϕ	diameter, m
ϕ_t	diameter of a truncating plane, m
τ	full width at half maximum of laser power peak, s

1. INTRODUCTION

Drag reduction technique with focused energy deposition into the flow ahead of a body in supersonic or hypersonic flows has been paid much attention recently. [1-3] A number of past works have shown

^aAssociate professor

that the aerodynamic drag force on the body can be reduced by supplying the energy of a laser pulse.[4-7] In the method, the drag decreases during the interaction of the low density and high temperature region created by the energy deposition with the shock wave over the body, depending on the laser parameters such as pulse repetition frequency, laser energy or duration time. Therefore, the effect of the energy supply on the drag reduction should be better understood in order to apply this technique practically.

Borzov et al. showed in their numerical study[8] that when a constant source of power is supplied ahead of a blunt body in a hypersonic flow of $M=10$, the drag is reduced more effectively for the blunt body with larger bluntness. For a lower Mach number, typically at $M=2$, such an effectiveness for a blunt body needs to be evaluated more carefully, because the nonlinear effect of energy deposition into flow on drag reduction becomes weaker. The drag for a blunt body obtained by energy deposition should be lower than that for a sharp cone with the same reference area without energy deposition at such supersonic speed from the standpoint of practical drag performance. In addition, the energy savings due to drag reduction should be large for effective energy usage.

Although the drag reduction with energy deposition is more effective for a blunt body with larger bluntness, the drag without energy deposition is relatively higher as bluntness is larger. The effective time, for which the effect of the energy deposition on a blunt body lasts, is a key parameter to know what shape of a body is better to obtain lower drag. In our recent study[9], the effective time is evaluated during the interaction of the low density core created by a single laser pulse using an Nd:YAG laser with the bow shock wave over a blunt body. The evaluated effective time for a flat-faced cylinder is longer than that for a hemisphere under the same energy deposition condition. The longer effective time for the flat-faced cylinder is due to the fact that the recirculation zone with vortices, which are produced due to baroclinic interaction, keeps for longer time in the forebody region. This trend results in the reduction of the drag for a longer period.[3] From our numerical study[10], however, it has shown that the modulated drag for the flat-faced cylinder is nearly the same with that for the hemisphere and that the drag value is higher than that for the sharp cone without energy deposition. Nevertheless, it is believed that flat-faced geometry has a potential advantage to be used in the drag reduction with energy deposition, because the energy savings for the flat-faced cylinder are higher than that for the hemisphere under the same energy deposition condition.

The lessons learned from the past studies lead to an idea to make the most of each characteristics of flat-faced cylindrical and conical geometry on the modulation of the drag with the energy addition: the drag value is reduced on the frontal portion of a body by keeping a vortex flow feature with flat-faced cylindrical geometry, while the drag on the base region is kept lower by using conical geometry. A truncated cone, which is proposed in this study for supersonic drag reduction with energy deposition, is expected to realize such performance.

In the present study, efforts are made to show better drag reduction performance using a truncated cone with repetitively pulsed laser energy depositions. A computational fluid dynamic (CFD) method is used to calculate the flow structure and the wave drag on the body for a set of the parameters such as the truncation of a cone, the repetitive frequency of laser pulse, the energy deposition position, and the amount of the energy supplied into flow. The issues on a system integration such as the weight penalty of the laser device for energy deposition are not considered in the present study.

In addition, viscous effect is ignored in the present calculations. Therefore, the heat transfer rate to the wall of the body, including detailed flow phenomena such as Edney IV interaction [5], is not accounted for in the evaluation of the supersonic drag performance. Basically, heat deposition will increase the heating rate to a body surface. In the present study, the drag for the sharp cone, the truncated cones with different truncating surface, and the flatfaced cylinder for the same diameter of the base are calculated. The sharper nosed body will increase the heating rate as compared with the blunt nosed body through the interaction of the high temperature cores created with energy deposition. This aspect needs to be estimated for the further details on drag performance. Such estimation is beyond the scope of the present study, and remains to be made in the future.

2. NUMERICAL METHOD

The 2d-axisymmetric inviscid flow over a body is assumed to be a perfect gas with the constant specific heat ratio of 1.4. Mass, momentum and energy conservation equations are discretized using a finite-volume method. The numerical flux function is evaluated using the AUSM-DV scheme. The MUSCL approach is employed with a minmod limiter, and computed flow properties are second-order accurate

in space. The discretized equations are numerically integrated in time by using a second-order Runge-Kutta method. It should be noted that the present CFD method can predict the time variation of the stagnation point pressure very well.[9] Thus, the validity of the method is believed to be warranted.

The parameters used in the present calculations are summarized in Table 1. The diameter of the base of the blunt body, ϕ , the diameter of the truncating plane, ϕ_t , and the distance upstream of a body to energy deposition position, s , are schematically shown in Fig. 1. The geometrical shapes with different ϕ_t/ϕ values are additionally shown in the same figure. The base diameter and the conical angle of the truncated cone are set to be 20mm and 30 degrees, respectively. A slip condition is imposed at the wall of the body.

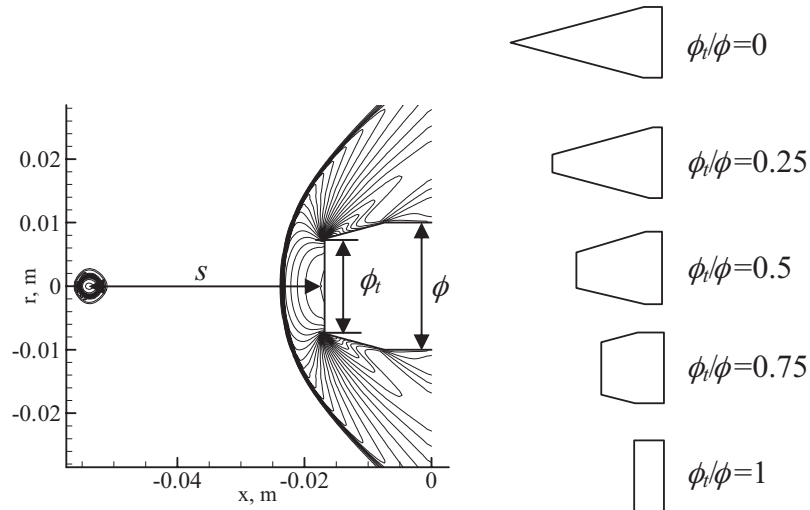


Figure 1. Simulation parameters and blunt bodies used in the present study.

Table 1. Summary of the simulated parameters

Parameter	Value
ϕ	20mm
f	10kHz, 50kHz, 100kHz
ϕ_t/ϕ	0, 0.25, 0.5, 0.75, 1
Q	3mJ, 4.5mJ, 6mJ
s/ϕ_t	2.0, 2.5, 2.667, 3.0, 3.5, 4.0

For all the cases analyzed in the present study, a steady-state solution is calculated for the case without energy deposition at first, and the unsteady calculation with energy deposition is carried out from the steady-state solution. The calculated drag value at its steady-state without energy deposition is shown in Fig. 2. In the figure, each drag value is normalized by the one for the flat-faced cylinder.

The Mach number and the static pressure are set to be 2 and 12.7kPa, respectively. The set of the values is taken from the condition for the specification of an indraft supersonic wind tunnel which will be used in our experiment planned in future. The static temperature in the freestream is calculated through an isentropic flow relation assuming that the total temperature of the freestream flow is taken to be 300 K. All the computed results are presented by using a 201×201 computational grid. A time step is set to be a constant value of 3ns. The sensitivity of the grid size and the time step to the calculated results is believed to be small, as will be shown later.

A heating source term for a periodic laser energy deposition is calculated assuming that the energy is deposited during the period of the order of the laser pulse duration at constant volume and that the deposited energy distribution is given by a Gaussian profile. A well-known formulation[11] for the energy deposition is used in the present study as follows:

$$S(x, y, t) = \lambda(t)q_0 \exp\left[-\frac{(x-x_0)^2 + r^2}{r_0^2}\right] \quad (1)$$

where $\lambda(t)$ denotes a step function with the full width of the half maximum τ ,

$$\lambda(t) = \begin{cases} 1, & 0 \leq \text{mod}(t, \frac{1}{f}) \leq \tau \\ 0, & \tau < \text{mod}(t, \frac{1}{f}) < \frac{1}{f} \end{cases} \quad (2)$$

The value of q_0 is given by the following relation:

$$q_0 = \frac{Q}{\tau \int_{v_0} \exp\left[-\frac{(x-x_0)^2 + r^2}{r_0^2}\right] dv} \quad (3)$$

where Q is a laser energy absorbed into flow. Note that $(x_0, 0)$ is a center of the spherical region for the energy deposition. The value of Q is set to be 3mJ, 4.5mJ, and 6mJ, respectively. These values in the range from 30% to 60% of a maximum laser energy per pulse (10mJ) for an Nd:YLF laser with the laser wavelength of 1,047nm[12]. The value of the absorbed energy volume, v_0 , is assumed to be the same value of 3 mm³ used in the past work.[9] The full width of half maximum for a pulse, τ , is given from the value for the Nd:YLF laser[12] and is taken to be 9 ns.

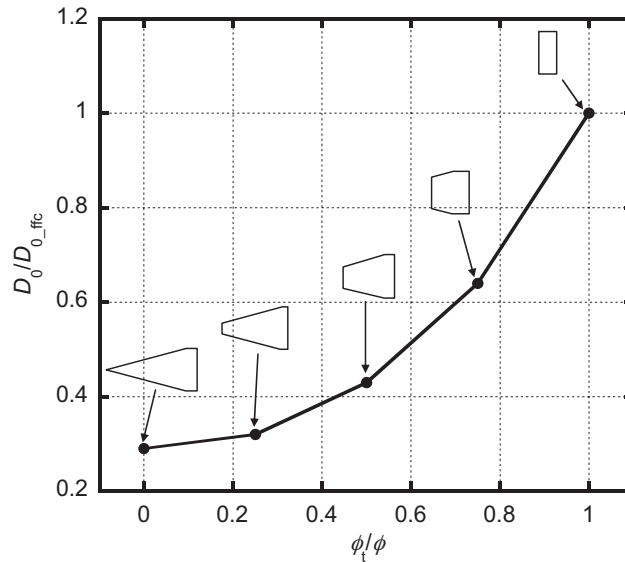


Figure 2. Comparison of the drag without energy deposition for the blunt bodies analyzed in the present study. Each of the drag values is normalized by the one for the flat-faced cylinder with $\phi_t/\phi=1$.

The volume value and the deposited energy used in the present study are believed to be reasonable. In our past work[9], the interaction of the low density region created by an Nd:YAG laser with the laser wavelength of 1,064 nm is simulated under the condition in which the Mach number and the static pressure are set to be 3 and 3kPa, respectively. The same volume value is used in our previous study. The amount of the energy deposited into the flow is estimated to be about 3.6mJ by fitting the measured blast wave evolution. It should be noted that the static pressure in the freestream in the present study is higher than that in the previous study. The laser energy deposited should be increased with pressure. We will examine these properties in our planned experiment with the Nd:YLF laser.

3. RESULTS AND DISCUSSION

3.1. Asymptotic Drag Characteristics

The convergence histories of the wave drag on the frontal surface of the body are given in Fig.3 for the three different repetitive frequencies of $f=10\text{kHz}$, 50kHz , and 100kHz , respectively. The drag is

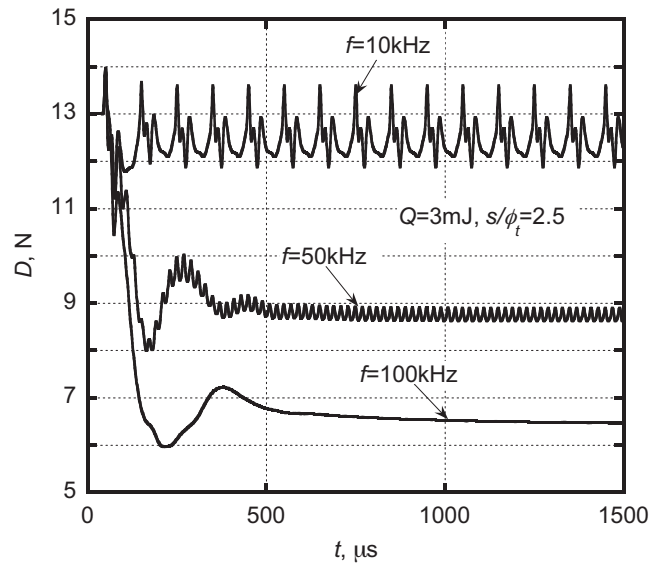


Figure 3. Convergence histories of the calculated drag on the frontal surface at $f=10\text{kHz}$, 50kHz , and 100kHz for the case of $\phi_t/\phi=0.75$, $Q=3\text{mJ}$, and $s/\phi_t=2.5$.

calculated by integrating the pressure on the frontal surface. The energy deposited and the normalized distance upstream of the body surface to energy deposited point are set to be $Q=3\text{mJ}$, and $s/\phi_t=2.5$, respectively.

As shown in Fig. 3, in each of the cases, the drag asymptotically approaches to a quasisteady state, showing periodical fluctuations. The drag value averaged between $t=1,400\mu\text{s}$ and $t=1,500\mu\text{s}$ is 12.4 N , 8.7 N , and 6.5 N , for the case of $f=10\text{kHz}$, 50kHz , and 100kHz , respectively: the ratio of the reduced drag to the one without energy deposition is about 96%, 67%, and 50%, respectively. For $f=10\text{kHz}$, the fluctuations are relatively large: the standard deviation from the averaged value is about $\pm 3.7 \times 10^{-1}\text{N}$. For $f=50\text{kHz}$, the drag becomes a quasi-steady state value within $500\mu\text{s}$. The standard deviation of the periodical fluctuation is about $\pm 9.5 \times 10^{-2}\text{N}$, which is smaller than that for $f=10\text{kHz}$. For the case of $f=100\text{kHz}$, a similar trend for $f=50\text{kHz}$ is seen, but the oscillation becomes weaker as compared with that for $f=50\text{kHz}$: the standard deviation is about $\pm 2.6 \times 10^{-3}\text{N}$. A similar tendency is seen in other simulated conditions, though the results are not shown here.

In Fig.4, the averaged drag values for the three truncated cones are plotted against the normalized energy deposition position, s/ϕ_t . The results are presented for the case of $Q=4.5\text{mJ}$. From the figure, the difference of the averaged drag value between the three truncated cones is about 4% at most. Thus, within the calculated results in the present study, the effect of the energy deposition position on the drag is believed to be weak. As shown, because the lowest drag value is obtained for the case of $s/\phi_t=2.5$, the results will be shown mainly for $s/\phi_t=2.5$ in later sections.

The effect of the truncating plane on the drag reduction is examined especially for the case of $f=100\text{kHz}$ by changing the deposited energy from $Q=3\text{mJ}$ to 6mJ . The averaged drag values are compared in Fig. 5 between the cases of $\phi_t/\phi=0.25$, 0.5 , and 0.75 . For reference, the sharp cone ($\phi_t/\phi=0$) and the flat-faced cylinder ($\phi_t/\phi=1$) are also shown in Fig. 5. Each of the drag values is averaged between the same time period mentioned earlier, respectively, except for the sharp cone: this case is convergent to a quasi-steady state quickly as compared with other cases, and the drag value is averaged between $t=400\mu\text{s}$ and $t=500\mu\text{s}$. The energy deposited position is set to be $s/\phi_t=2.5$ for all the cases. For additional reference, an analytical drag of the sharp cone without energy deposition is shown also in the figure: the drag value is evaluated based on the Taylor-Maccoll solution[13].

From Fig. 5 for the case of $Q=3\text{mJ}$, the drag value becomes lower as the truncation surface is decreased: the difference of the drag value between $\phi_t/\phi=0.25$ and 0.75 is about 10%. The drag value for $\phi_t/\phi=0.25$ is lower than the analytical drag for the sharp cone. Note that the ratio of the reduced drag to the one without energy deposition is about 89%, 69%, and 50% for the case with $\phi_t/\phi=0.25$, 0.5 , and 0.75 , respectively.

One can see in Fig. 5 that by increasing the deposited energy up to $Q=6\text{mJ}$, the drag with the larger truncation surface is reduced more strongly: the difference of the drag between with $Q=3\text{mJ}$ and $Q=6\text{mJ}$ is about 10% for the case of $\phi_l/\phi = 0.75$, and is about 3% for $\phi_l/\phi = 0.25$. At $Q=6\text{mJ}$, the drag values for all the truncated cones are smaller than the analytical value.

Calculation is made with a 201×401 computational grid for the case with $\phi_l/\phi = 0.75$, $Q=3\text{mJ}$, and $f=100\text{kHz}$. The calculated averaged drag value is increased by about 0.8% as compared with that obtained with the 201×201 grid. In addition, calculation is performed with the time step size of 1ns. The difference of the averaged drag value between the step size of 3ns and of 1ns is found to be less than 0.1%.

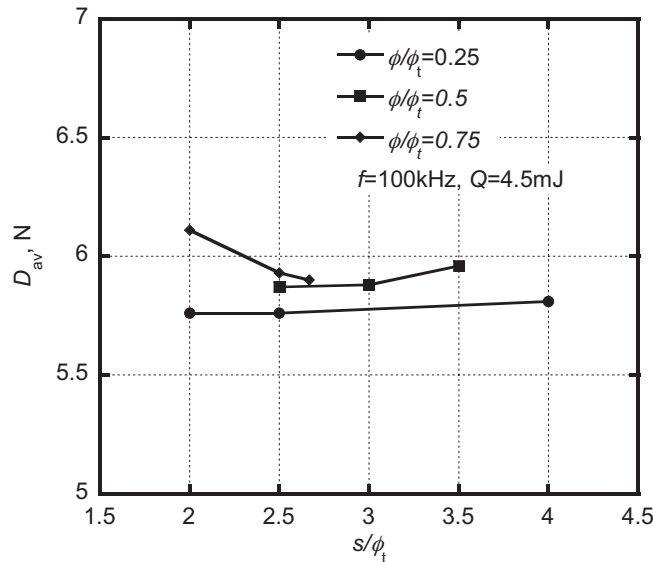


Figure 4. Effect of energy deposition position on the averaged drag for the case of $f=100\text{kHz}$, and $Q=4.5\text{mJ}$.

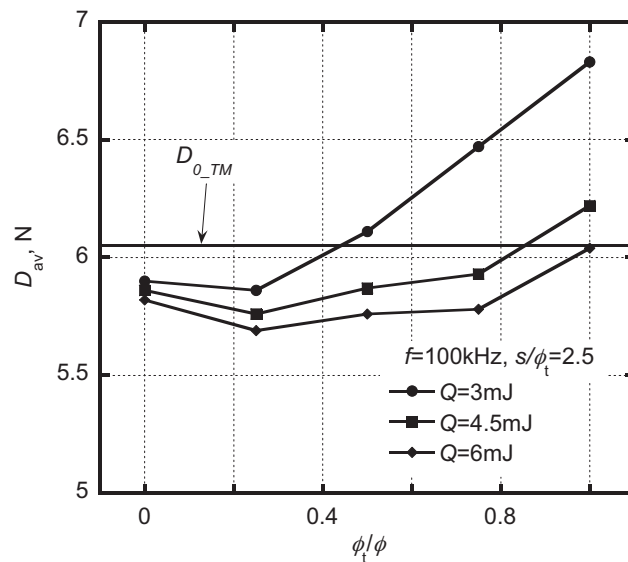


Figure 5. Effect of the truncated geometry on the drag reduction for the case of $f=100\text{kHz}$, and $s/\phi_t = 2.5$.

3.2. Quasi-Steady State Flowfield

The calculated quasi-steady flowfield will be presented in this subsection. The flowfield is qualitatively different between the lower repetitive frequency at $f=10\text{kHz}$, and the higher frequencies at $f=50\text{kHz}$ and 100kHz . For the purpose of the comparison of the flowfield, the emphasis is placed on the difference

of the interaction pattern of the heated low density core with the bow shock wave. It should be noted that the results are given mainly for the case of $\phi_l/\phi=0.75$, $s/\phi_l=2.5$, and $Q=3\text{mJ}$, because the qualitative nature of the flowfield is unchanged for other cases.

3.2.1. $f=10\text{kHz}$

Figures 6 shows the density contours and instantaneous streamlines between $t=1,010\mu\text{s}$ and $t=1,110\mu\text{s}$, respectively. In Fig. 6(a), a blast wave and a low density core are approaching to the truncated cone. The blast wave and the low density core are produced during the energy deposition at $t=1,000\mu\text{s}$. The temperature in the low density core is about a couple of thousands Kelvin, though the result is not shown here. The low density core created at the previous energy deposition still stays near the corner of the truncated surface. From the streamline shown in Fig. 6(a), one can see vortices near the frontal surface of the body. The vortices are produced by the interaction of the bow shock wave and the low density core, as will be seen next. The vortex flow feature in the forebody region keeps for about $60\mu\text{s}$, resulting in the reduction of the drag on the frontal surface of the body, as is shown in Fig. 3.

One can see from the density contour in Fig. 6(b) at $t=1,050\mu\text{s}$ that the blast wave reaches at the frontal surface of the truncated cone. This feature is recognized as the sharp peak seen in Fig. 3. The low density core starts to interact with the bow shock wave. From the density contour at $t=1,080\mu\text{s}$ given in Fig. 5(c), the core is deformed by passing through the bow shock wave. The shape of the bow shock wave near the centerline is slightly distorted: the distortion is believed to be due to the decrease of the local Mach number in the density core.[6]

The streamline at $t=1,050\mu\text{s}$ shown in Fig. 6(b) indicates that the vortices observed at $t=1,010\mu\text{s}$ shown in Fig. 6(a) break down. By judging with the density contour in Fig. 6(b), one can find that the vortex flow structure cannot keep in the frontal region over the body until the low density core produced at the next deposition reaches near the bow shock wave under this repetitive frequency condition. As shown in Fig. 6(c), new vortices are produced in the region where the low density core passes through the shock wave. The vortices are generated due to the baroclinic effect followed by the interaction of the shock wave with the high temperature region.[14]

The deformed low density core moves downstream by spreading in the radially outward direction, as shown in Fig. 6(d). The shape of the bow shock wave is returns to its steady-state one. From the streamline given in Fig. 6(d), the flow velocity in the forebody region becomes opposite to the direction of the freestream flow. This reversal flow is mainly due to the fact that the pressure near the wall region is instantaneously higher than the one behind the bow shock: such a flow state is a result of the penetration of the low density core into the shock layer and the reflection of the blast wave at the wall. The reversal flow weakens in the next $30\mu\text{s}$ from $t=1,080\mu\text{s}$. The flow structure at $t=1,110\mu\text{s}$ shown in Fig. 6(e) is almost the same with the one at $t=1,010\mu\text{s}$ given in Fig. 6(a), as expected.

3.2.2. $f=50\text{kHz}$

Figures 7 shows the density contours and the instantaneous streamlines between $t=1,005\mu\text{s}$ and $t=1,025\mu\text{s}$, respectively. From the density contour at $t=1,005\mu\text{s}$ given in Fig. 7(a), one can see an oblique shock wave in the frontal region of the truncated cone. The oblique shock wave is formed through the interaction of the low density core with the bow shock wave, as seen in the case at $f=10\text{kHz}$. In contrast to the lower repetitive frequency, the bow shock wave is strongly distorted at $f=50\text{kHz}$ due to the multiple density cores incoming into the forebody region of the body, as can be seen in Fig. 7(a). The shape of the oblique shock wave is nearly constant even if the low density core interacts with the shock wave successively, as shown in Figs. 7(a) to 7(e).

A relatively large vortex flow region is produced due to the baroclinic effect through the successive interaction of the low density cores with the shock wave. The resultant flowfield shows a recirculation zone. As shown in the streamlines in Figs. 7(a) to 7(e), the recirculation zone is maintained in the frontal region of the body. The observed streamline shows a strong similarity with the one over a pure cone in supersonic flow: the recirculation zone serves as virtual conical geometry in the flowfield, blocking the supersonic flow incoming to the body.[1] Because the low density core flows through the recirculation zone in the forebody region, the pressure on the truncated surface is kept lower as compared with the case at $f=10\text{kHz}$. However, as shown in Fig. 7(b), the blast wave collides with the truncated surface. The collision represents the increase in the time history of the drag shown in Fig. 3.

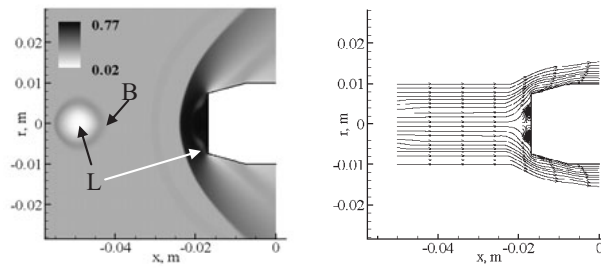
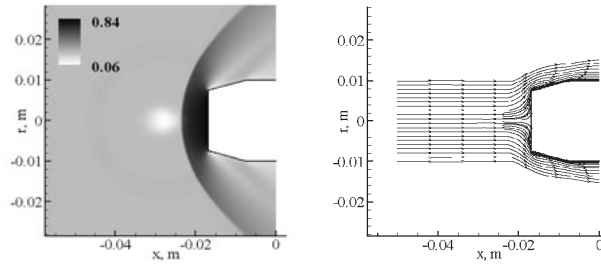
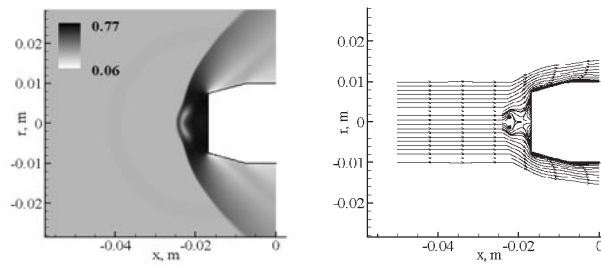
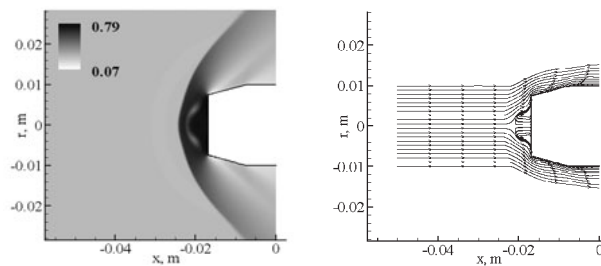
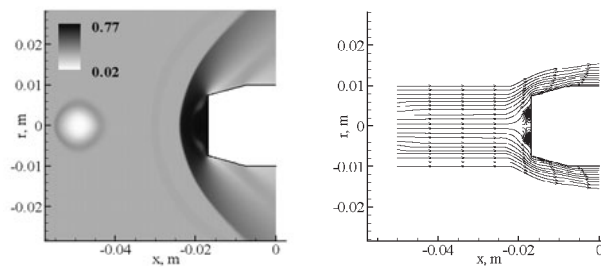
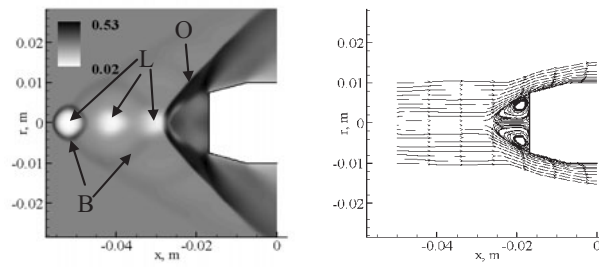
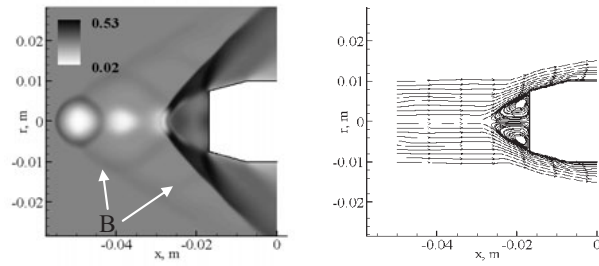
(a) $t=1,010$ s (B: blast wave, L: low density core)(b) $t=1,050$ s(c) $t=1,070$ s(d) $t=1,090$ s(e) $t=1,110$ s

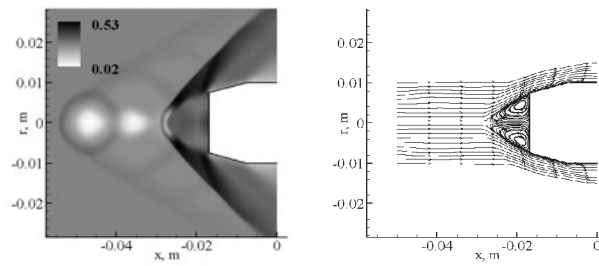
Figure 6. Flowfield structure between $t=1,010\mu\text{s}$ and $t=1,110\mu\text{s}$ at $f=10\text{kHz}$, $s/\phi_t=2.5$, $Q=3\text{mJ}$, and $\phi_t/\phi=0.75$, left side: density contour, and right side: instantaneous streamline.



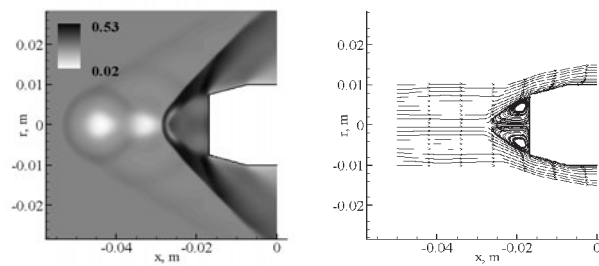
(a) $t=1,005$ s (B : Blast wave, L : Low density core, O: oblique shock wave)



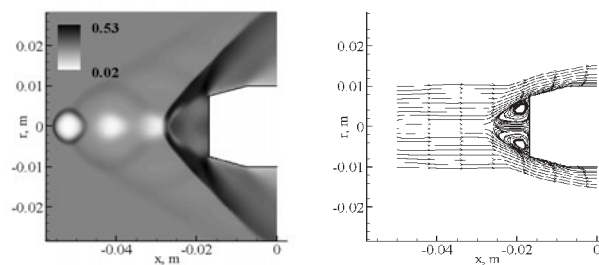
(b) $t=1,010$ s



(c) $t=1,015$ s



(d) $t=1,020$ s



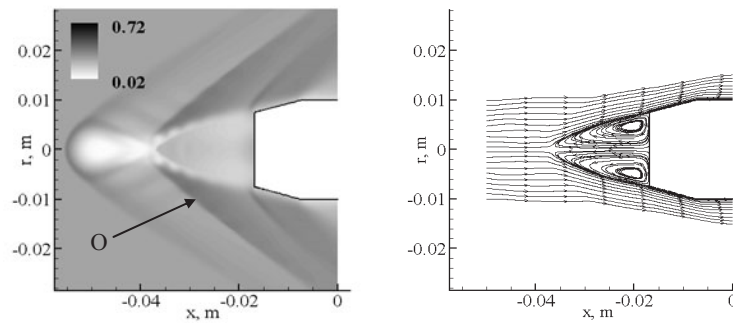
(e) $t=1,025$ s

Figure 7. Flowfield structure between $t=1,005\mu\text{s}$ and $t=1,025\mu\text{s}$ at $f=50\text{kHz}$, $s/\phi_t=2.5$, $Q=3\text{mJ}$, and $\phi_t/\phi=0.75$, left side: density contour, and right side: instantaneous streamline.

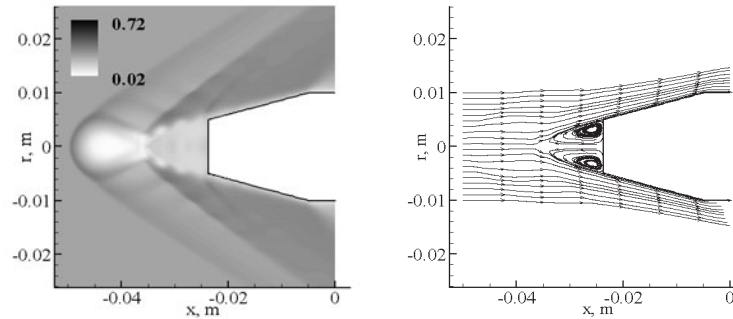
3.2.3. $f=100\text{kHz}$

The density contour and the streamline at $t=1,010\mu\text{s}$ is shown for the case of $\phi_t/\phi=0.75, 0.5,$ and 0.25 in Figs. 8(a), 8(b), and 8(c), respectively. From the comparison of the results, the recirculation zone is formed similarly in the frontal region of the body for each of the cases. The size of the recirculation zone becomes smaller as the truncated surface is reduced. The apex of the recirculation zone is estimated from the obtained solution by searching the position where the sign of the axial flow velocity on the centerline is changed. The position of the apex is about 20mm, 12mm, and 3mm upstream of the body surface for $\phi_t/\phi=0.75, 0.5,$ and $0.25,$ respectively. It should be noted that the effect of the drag reduction between with and without energy deposition becomes stronger as the truncated surface is increased. Thus, the recirculation zone due to baroclinic interaction is a key phenomenon to obtain the reduced drag for the case with larger truncating surface.

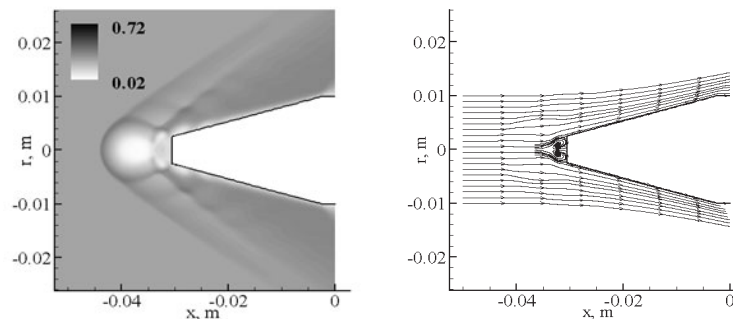
From the comparison of the density contours with $\phi_t/\phi=0.75$ between $f=100\text{kHz}$ and $f=50\text{kHz},$ as shown in Figs 8(a), and Fig. 7, respectively, the angle of the oblique shock wave for $f=100\text{kHz}$ is shallower than that for $f=50\text{kHz}.$ This trend is due to the fact that the size of the recirculation zone is larger for $f=100\text{kHz}$ as compared with the one for $f=50\text{kHz}.$ As a result, the forebody region over the



(a) $\phi_t/\phi=0.75$ (O: oblique shock wave)



(b) $\phi_t/\phi = 0.5$



(c) $\phi_t/\phi = 0.25$

Figure 8. Quasi-steady flowfield, $s/\phi_t=2.5,$ $Q=3\text{mJ},$ and $f=100\text{kHz},$ left side: density contour, and right side: instantaneous streamline.

truncated cone is maintained at a lower pressure level, and the collision of the blast wave contributes to the increase of the drag only slightly. Such a feature can be related to the smaller oscillation at $f=100\text{kHz}$ shown in Fig. 3, as compared with those for the lower repetitive frequencies.

3.3. Trade-off Between Energy Savings and Drag

Figure 9 shows that the time history of an energy saving efficiency, which is given by the ratio of the energy savings due to drag reduction to the sum of the repetitively supplied energy:

$$\text{Efficiency} = \frac{\int V_{\infty} (D_0 - D) dt}{\sum Q} \quad (4)$$

The efficiency value is plotted against the time for the case of $\phi_l/\phi=0.75$, $s/\phi_t=2.5$ and $Q=3\text{mJ}$ at $f=10\text{kHz}$, 50kHz , and 100kHz , respectively.

One can see from the figure that each of the efficiency values increases gradually and reaches its asymptotes nearly up to $t=1,500\mu\text{s}$. The efficiency values averaged between $t=1,400\mu\text{s}$ and $t=1,500\mu\text{s}$ are in the range of from 10 to 15. When the deposition energy is increased up to $Q=6\text{mJ}$ at $f=100\text{kHz}$, the obtained efficiency is about 6, which is still higher than 1, though the result is not shown here. It should be noted that the efficiency values for the other cases calculated in the present study asymptote similarly as in Fig. 9.

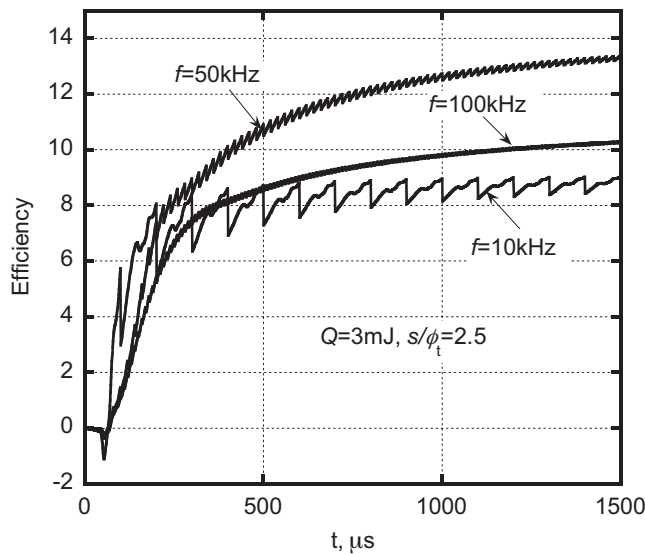


Figure 9. Convergence histories of the efficiency at $f=10\text{kHz}$, 50kHz , and 100kHz for the case of $\phi_l/\phi=0.75$, and $s/\phi_t=2.5$.

In Fig. 10, the averaged efficiency is plotted against the averaged drag value for the cases of $\phi_l/\phi=0.25$, 0.5 , and 0.75 with $s/\phi_t=2.5$, respectively. The results are presented for $Q=3\text{mJ}$, 4.5mJ , and 6mJ , respectively. For the purpose of comparison, two dashed lines are given to show the analytical drag value for the sharp cone without energy deposition, and the efficiency value of 1, respectively. For reference, the calculated results for the sharp cone ($\phi_l/\phi=0$) and the flatfaced cylinder ($\phi_l/\phi=1$) are given in the same figure.

From the figure, for the flat-faced cylinder ($\phi_l/\phi=1$), the efficiency value is higher as compared with the other cases, while the averaged drag value is typically higher than the analytical drag for the sharp cone. For the cases of the truncated cone with $\phi_l/\phi=0.5$ and 0.75 , the drag values can be lower than the analytical one for $Q=4.5\text{mJ}$, and 6mJ , respectively, keeping the efficiency values higher than 1. In contrast, although the drag values for the truncated cone with $\phi_l/\phi=0.25$ are consistently lower than the analytical one, the efficiencies are nearly equal to or is lower than 1. One can see that the efficiency value for the sharp cone ($\phi_l/\phi=0$) is lower than 1; the drag values are lower than the analytical one under the conditions analyzed in the present study. Thus, it is believed that the truncated cone with larger flat surface shows good trade off performance between the energy savings and the modulated drag.

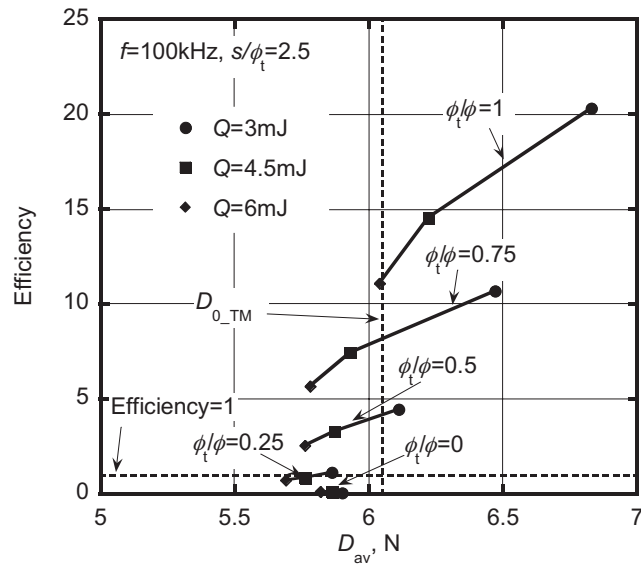


Figure 10. Effect of the truncated geometry on the averaged drag and efficiency for the case of $f=100\text{kHz}$, and $s/\phi_t=2.5$.

4. CONCLUSIONS

The present numerical study demonstrates the functions of a truncated nose of a supersonic flying body with repetitive energy depositions. The wave drag over the truncated cone can be reduced effectively by setting the parameters on the energy deposition appropriately: by increasing the repetitive frequency, the drag is reduced, and the oscillation of the drag is decreased; however, the efficiency decreases by increasing the energy deposited into flow. The drag for a truncated cone can be smaller than that for a sharp cone with the same apex angle. The present result shows that the drag reduces as the truncating surface area is decreased; in contrast, the efficiency is higher as the surface area increases. Based on the obtained trend in the present study, the truncated cone with a moderate frontal surface could be a better choice for the drag reduction technique with energy deposition.

A quasi-steady state flowfield over truncated conical geometry is established with the higher repetitive frequency of pulse energy, typically higher than $f=50\text{kHz}$ for the body with $\phi=20\text{mm}$. The quasi-steady state flowfield shows the recirculation zone over the truncated body surface. The formation of the conical recirculation zone serves as a virtual spike over the body. The size of the recirculation zone gives the overall pressure level in the forebody region of the truncated cone. The production of the vortices due to baroclinic effect governs the stabilization of the recirculation zone.

ACKNOWLEDGEMENT

The author would like to thank Profs. Akihiro Sasoh, and Atsushi Matsuda, and Mr. Yohei Sekiya of Nagoya University for their helpful suggestions throughout this work.

REFERENCES

1. Riggins D., Nelson H. F., and Johnson E., "Blunt-Body Wave Drag Reduction Using Focused Energy Deposition," *AIAA Journal*, Vol. 37, No. 4, 1999, pp. 460-467.
2. Kremeyer K., Sebastian K., and Shu C. W., "Computational Study of Shock Mitigation and Drag Reduction by Pulsed Energy Lines," *AIAA Journal*, Vol. 44, No. 8, 2006, pp. 1720-1730.
3. Taguchi S., Ohnishi N., Furudate M., and Sawada K., "Numerical Analysis of Drag Reduction for Supersonic Blunt Body by Pulse Energy Deposition," AIAA Paper 2007-1235, January 2007.
4. Tret'yakov P.K., Garanin A. F., Grachev G. N., Krainev, V. L., Ponomarenko A. G., Tishchenko V. N., and Yakovlev, V. I., "Control of Supersonic Flow around Bodies by Means of High-Power Recurrent Optical Breakdown," *Physics-Doklady*, Vol. 41, Issue 11, 1996, pp. 566-567.
5. Adelgren, R. A., Yan, H., Elliott G. S., Knight D. D., Beutner T. J., and Zheltovodov, A. A., "Control of Edney IV Interaction by Pulsed Laser Energy Deposition," *AIAA Journal*, Vol. 43, No. 2, 2005, pp. 256-269.

6. Georgievsky, P., and Levin, V., "Unsteady Interaction of a Sphere with Atmospheric Temperature Inhomogeneity at Supersonic Speed," *Mekhanika Zhidkosti i Gaza*, No.4, May-June 1993, pp.174-183 (in Russian); translated in *Fluid Dynamics*, Vol. 28, No. 4, 1993, pp.568-574.
7. Knight D., Kuchinskiy V., Kuranov, A., and Sheikin, E., "Survey of Aerodynamic Flow Control at High Speed By Energy Deposition," AIAA Paper 2003-0525, January, 2003.
8. Borzov V. Y., Rybka I.V., and Yur'ev A. S., "Effect of Local Energy Supply To a Hypersonic Flow On the Drag of Bodies With Different Nose Bluntness," *Journal of Engineering Physics and Thermophysics*, Vol. 67, Nos. 5-6, 1994, pp. 997-1002.
9. Sakai T., Sekiya Y., Mori K., and Sasoh A., "Interaction Between Laser-Induced Plasma and Shock Wave Over a Blunt Body in a supersonic flow," Proceedings of the Institution of Mechanical Engineers, Vol. 222, Part G, *Journal of Aerospace Engineering*, 2008, pp. 605-617.
10. Sakai T., Sekiya Y., Mohd Rizal B. R., Matsuda A., Sasoh, A., "Unsteady Interaction of Blunt Bodies With Laser Induced Plasma in A Supersonic Flow," AIAA-Paper 2008-3794, Seattle, WA. June, 2008..
11. Zheltovodov, A. A., Pimonov, E. A., and Knight D.D., "Energy Deposition Influence on Supersonic Flow Over Axisymmetric Bodies," AIAA Paper 2007-1230, January, 2007.
12. Matsuda A., Sekiya Y., Rizal Rosli M., Sakai T., and Sasoh A., "Plasma Behavior Induced by Repetitive Laser Pulses," AIAA Paper 2008-3898, June 2008.
13. Sims J., "Tables for Supersonic Flow Around Right Circular Cones at Zero Angle of Attack," NASA-SP-3004, March, 1964.
14. Sasoh, A, Ohtani, T., and Mori, K., "Pressure Effects in a Shock-Wave-Plasma Interaction Induced by a Focused Laser Pulse," *Physical Review Letters*, Vol. 97, No. 20, Art.No. 205004, November 2006.

